Cell, Vol. 113, 743–753, June 13, 2003, Copyright ©2003 by Cell Press

A Kinesin, InvA, Plays an Essential Role in *Volvox* Morphogenesis

Ichiro Nishii,[1] Satoshi Ogihara,[2] and David L. Kirk[1,*]

[1]Department of Biology
Washington University
St. Louis, Missouri 63130

[2]Department of Biology
Graduate School of Science
Osaka University
Toyonaka, Osaka 560
Japan

Summary

In *Volvox carteri* adults, reproductive cells called gonidia are enclosed within a spherical monolayer of biflagellate somatic cells. Embryos must "invert" (turn inside out) to achieve this configuration, however, because at the end of cleavage the gonidia are on the outside and the flagellar ends of all somatic cells point inward. Generation of a bend region adequate to turn the embryo inside out involves a dramatic change in cell shape, plus cell movements. Here, we cloned a gene called *invA* that is essential for inversion and found that it codes for a kinesin localized in the cytoplasmic bridges that link all cells to their neighbors. In *invA* null mutants, cells change shape normally, but are unable to move relative to the cytoplasmic bridges. A normal bend region cannot be formed and inversion stops. We conclude that the InvA kinesin provides the motile force that normally drives inversion to completion.

Introduction

Curling of a cellular sheet is a versatile and widely employed shape-generating mechanism that is involved in metazoan gastrulation, neurulation, and many aspects of organogenesis. The cellular and molecular changes that underlie such morphogenetic events in metazoans are often complex, however (Schock and Perrimon, 2002), involving changes in cell number, shape, adhesion, arrangement, and state of differentiation. They are often different in the different cellular regions (Kiehart et al., 2000). Disentangling all of these interacting processes has proven challenging, and dissection of the genetic program underlying such a morphogenetic event has barely begun.

Inversion in the multicellular green alga *Volvox carteri*—in which an embryo consisting of a spherical cellular monolayer turns itself completely inside out—provides a simpler model system for analyzing both the subcellular mechanisms and the genetic program for curling of a cell sheet (Kirk, 1998, 1982; Kirk and Nishii, 2001). The resemblance of inversion to gastrulation has been noted ever since inversion was discovered (Kuschakewisch, 1923), and this apparent similarity was reinforced when it was found that inversion involves "flask cells" (Kelland, 1977; Viamontes and Kirk, 1977) like those seen at the dorsal lip of the amphibian blastopore.

Volvox carteri adults are "spheroids" with many small, biflagellate somatic cells on the surface and a few large asexual reproductive cells, or "gonidia," just below the surface (Figure 1A). However, in a *Volvox* embryo at the end of cleavage the gonidia are on the outside and the flagellar ends of somatic cells are on the inside, so inversion is required to establish the adult configuration (Starr, 1969). Detailed analysis of inversion led to the following view. Generation of the acute bend region where the cell sheet turns inside-out involves two coordinated activities: (1) cells near the bend region become "flask-shaped," with long, thin stalks at their outer ends, and (2) flask cells enter the bend region by moving inward individually, relative to the network of cytoplasmic bridges that links them to their neighbors. As the cells go from being linked by these bridges at their widest points to being linked at their thin outermost ends, the cell sheet is forced to curl sharply outward (Green et al., 1981; Viamontes et al., 1979).

Cytoskeletal elements have been strongly implicated in the inversion process. The flask-cell shape depends on numerous cortical microtubules that originate near the basal bodies and traverse the entire cell, passing close to the cytoplasmic bridges (Viamontes et al., 1979). Early studies suggested that movement of cells into the bend region was actin-dependent (Viamontes et al., 1979), but a more recent study suggests that actin and myosin play a role that facilitates propagation, but not initial formation, of the bend (Nishii and Ogihara, 1999). The roles of motor and regulatory proteins have been awaiting investigation.

The attractiveness of *V. carteri* as a model for studying genetic programming of such a morphogenetic process was recognized when it was found that a quarter of the mutants recovered in the first mutational study of *Volvox* had inversion defects (Sessoms and Huskey, 1973). This notion was reinforced by a later study in which 60 mutants with various inversion defects were recovered (Kirk et al., 1982). Detailed analysis of such mutants foundered, however, because inversion defects prevented mating and Mendelian analysis, and methods for defining the primary molecular defects in the mutants could not be found.

The present study combines old and new methods to exploit the advantages of *V. carteri* as a developmental-genetic model for studying morphogenesis. As was first done 30 years ago, phototactic selection was used to enrich for inversion mutants and others that are unable to swim directionally (Sessoms and Huskey, 1973). But instead of chemical mutagenesis, we used low-temperature cultivation, which activates the *Volvox* transposon *Jordan* and generates transposon-tagged mutants (Kirk et al., 1999; Miller and Kirk, 1999). Temperature-inducible transposition of *Jordan* makes it possible to isolate mutants that both are stable at normal culture temperature and capable of being reverted at lower temperature.

Here, we used *Jordan* to tag and recover *invA*, a gene

*Correspondence: kirk@biology.wustl.edu

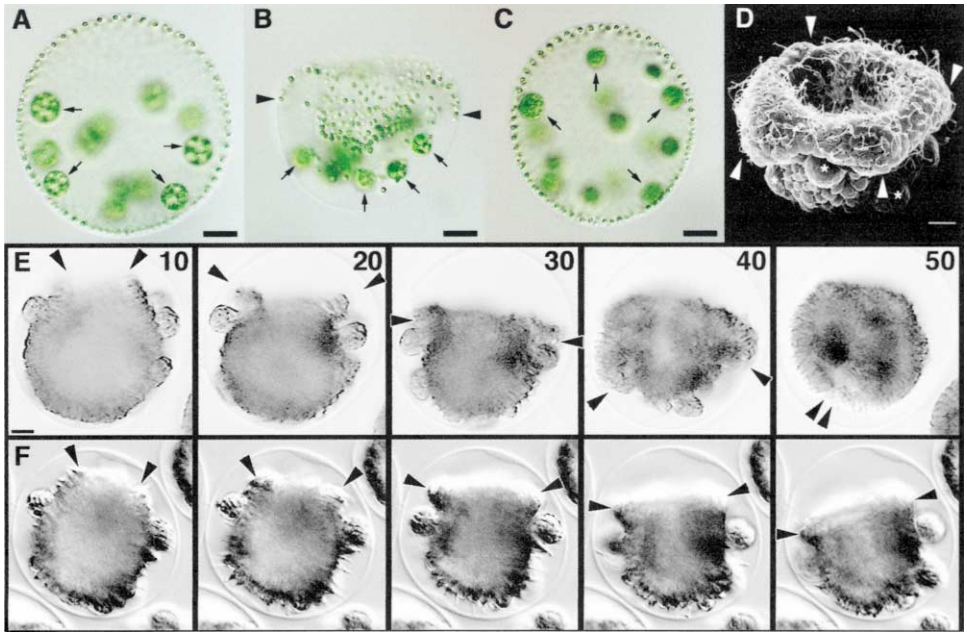

Figure 1. The Inversionless Phenotype of InvA

(A–C) Young adults of three related strains of *V. carteri*: (A) CRH22, the progenitor of InvA, (B) InvA, and (C) a wild-type revertant of InvA. In wild-type individuals (A and C), the gonidia (asexual reproductive cells; small arrows) are completely surrounded by a spherical monolayer of small somatic cells. However, in InvA (B), the gonidia are not surrounded by the somatic-cell layer because inversion of the embryo stopped when the edges of the somatic-cell layer reached the points indicated by the arrowheads. Scale bar is equal to 50 μm.

(D) An InvA individual several hours after inversion arrest. Arrowheads point to the four lobes of cells that initiated inversion but then stopped. Asterisks indicate gonidia. Although flagella develop and beat normally, InvA individuals cannot swim directionally. Scale bar is equal to 5 μm.

(E–F) Time-lapse video microscopy of wild-type embryos (E) and InvA embryos (F) during the inversion period. Arrowheads track the progress of inversion by pointing to the edges of the somatic-cell sheet. In the wild-type embryos, inversion is completed 45–50 min after it began. In InvA embryos, inversion appears to begin normally, but then it stops abruptly at about 30 min. The numbers indicate time after inversion started (min). Scale bar is equal to 10 μm.

that encodes a kinesin that is required for the completion of inversion. We then show that the InvA kinesin is associated with cytoplasmic bridges throughout inversion, and that inversion stops in *invA* mutants because the cells fail to move relative to their cytoplasmic bridges. This suggests to us that it is the InvA kinesin located in the cytoplasmic bridges that normally drives the cell movements that are required to complete inversion.

Results

Isolation of a Transposon-Tagged Inversion Mutant, InvA

By incubating the morphologically wild-type *V. carteri* strain, CRH22, at 24°C (which activates the *Jordan* transposon; Miller et al., 1993), then using unidirectional light to enrich for nonphototactic mutants (Sessoms and Huskey, 1973), and screening the resulting population microscopically, we isolated ~50 independent mutants with inversion defects. Ten of these reverted more frequently at 24°C than at 32°C, which is a feature of many *Jordan*-induced mutations. All ten mutants were screened on DNA blots for *Jordan* RFLPs not present in CRH22, or any of their revertants. One strain with a *Jordan* fragment of this sort, InvA, was selected for study.

InvA adults are "hat-shaped," with the somatic cells of the anterior hemisphere forming the brim, those of the posterior hemisphere forming the crown, and the gonidia dangling on the outside like ornaments (Figures 1B and 1D). This mutant phenotype, sometimes called "quasi-inversionless," has been observed before (Kirk et al., 1982; Sessoms and Huskey, 1973). Although the flagella on InvA somatic cells beat normally, the mutants spin in place instead of swimming directionally. We have not identified other significant effects of the *invA* mutation beyond its primary effect on inversion and its secondary effect on directional swimming.

Time-lapse video microscopy was used to compare the behavior of wild-type and InvA embryos during the inversion period (Figures 1E and 1F). The "phialopore"—the intersecting pair of slits at the anterior end of the embryo where inversion begins—opened normally in InvA and the lips of cells adjacent to the phialopore began to curl back over the rest of the embryo as in wild-type (Figures 1E and 1F; compare 10 and 20 min frames). But by 30 min, the curling of the cell sheet had stopped in the mutant, whereas it continued in wild-type embryos until the somatic-cell layer had completely surrounded the gonidia and the phialopore lips had come back together.

Inversion Stops in InvA Because Cells Fail to Move Relative to the Cytoplasmic Bridges

To understand the developmental defect in InvA, it is necessary to understand the role that a coherent net-

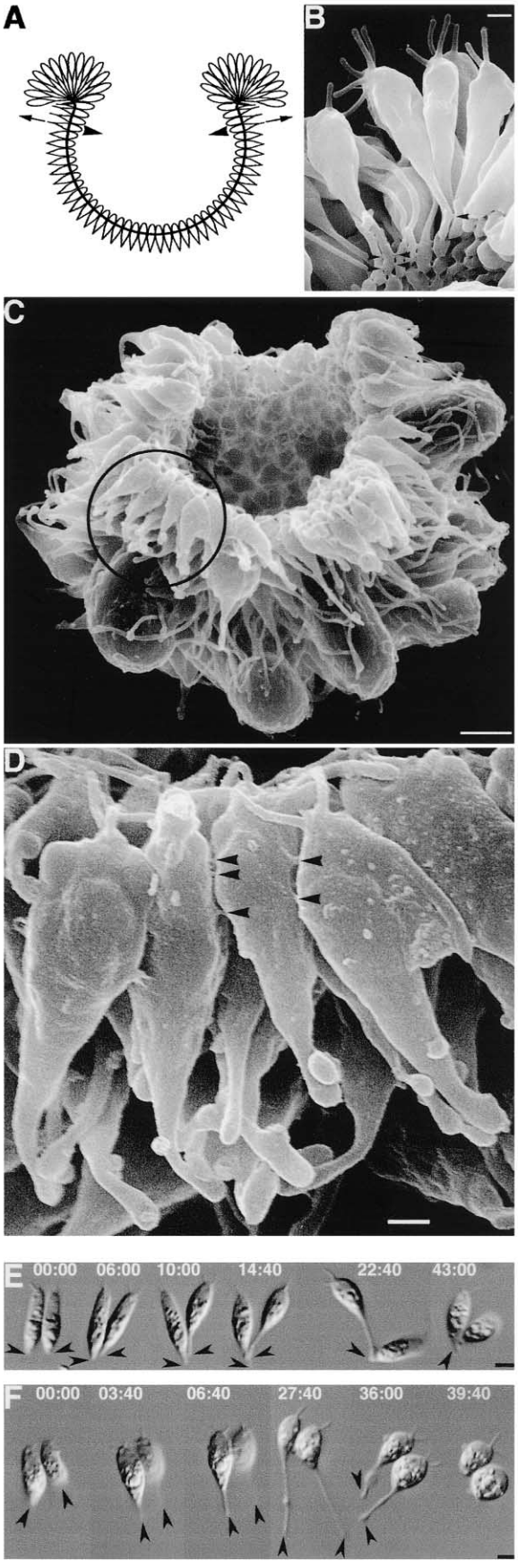

work of cytoplasmic bridges plays during inversion (Green et al., 1981). From the beginning of cleavage until well after the end of inversion, every cell of a *V. carteri* embryo is linked to its neighbors by numerous cytoplasmic bridges that form as a result of incomplete cytokinesis and that are highly regular in ultrastructure, size, and spacing. By the end of cleavage each cell is linked to its neighbors by a band of ~25 such bridges that girdle it near its equator, and the bridge bands of all cells in the embryo are interconnected and aligned to form a single, coherent network, or "cytoplasmic bridge system" (Figure 2A). This network of interconnected bridges holds the embryo together and provides the only structural framework against which cells can exert force to make the cell sheet bend outward.

The "bend region" where the cell sheet curls backward over itself is formed and propagated as a result of two activities of cells in that vicinity: (1) the cells form long thin "stalks" at their outer ends, and (2) they move inward relative to their cytoplasmic bridges. (The bridges cannot move because they are part of a coherent, interconnected cytoplasmic bridge network that runs through

Figure 2. SEM Analysis of the Inversion Defect in InvA

(A) A model, adapted from Green et al. (1981) indicating how it is believed that the force necessary to turn a *Volvox* embryo inside out is generated. The opening at the top of this diagrammatic cross-section of a wild-type embryo is called the phialopore. The continuous line running through the embryo represents the "cytoplasmic bridge system" that has been produced as a result of incomplete cytokinesis, and that is known to be the only thing holding the embryo together during inversion. The cytoplasmic bridge system links the spindle-shaped preinversion cells at their widest points. Cells that are about to enter the bend region of the inverting embryo undergo two changes: they become "flask-shaped" by producing long cytoplasmic extensions at their outer ends (outward pointing arrows), and they move inward relative to the cytoplasmic bridge system (inward-pointing arrowheads). As the cells go from being linked at their widest points to being linked at their slender, outermost tips, the cell sheet is forced to curl outwards sharply.

(B) Flask cells in the bend region of a wild-type embryo illustrating the fact that at this stage the cytoplasmic bridges linking the cells are located near the tips of the stalks (arrowheads). Scale bar is equal to 1 μm.

(C) An InvA mutant embryo fixed just after inversion arrest. The phialopore has opened, the cells have become flask-shaped, and the portion of the cell sheet surrounding the phialopore has curled outward to some extent. Scale bar is equal to 5 μm.

(D) Magnified image of the region encircled in (C). Although the cells have become flask-shaped, they have not moved relative to their cytoplasmic bridges (arrowheads), and so they remain linked to one another at their widest points. Scale bar is equal to 1 μm.

(E and F) Time lapse analysis of behavior of isolated cell pairs. Time is given as min:sec and arrowheads point to the outermost tips of the cells.

(E) Wild-type. The sequence begins while the cells are still in their preinversion, spindle-shaped state. The cells become flask-shaped by forming long slender stalks at their chloroplast ends and move sequentially relative to their common attachment point: their shared band of cytoplasmic bridges. By 22:40, the two cells are connected only at their outermost tips; at 43:00, after both cells have assumed their postinversion shapes, they remain attached at the tips.

(F) InvA both cells extend long stalks and become flask shaped as in wild-type. But movement relative to their common attachment point (the cytoplasmic bridge band) never occurs as it does in wild-type. Therefore, by the time the cells begin to assume their postinversion shapes at 39:40 they are still attached at the cell equator, just as they were initially. Scale bars are equal to 3 μm.

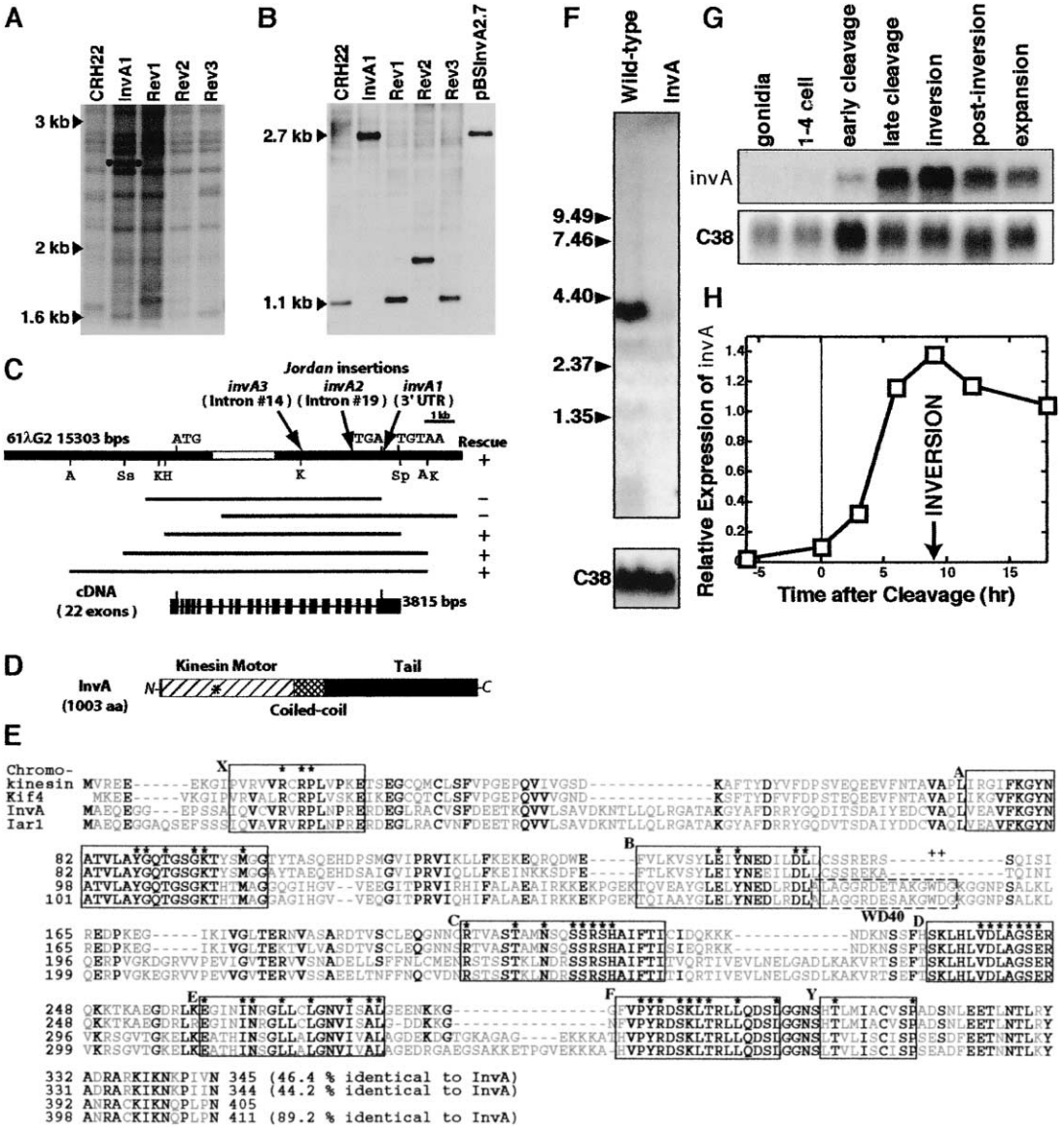

Figure 3. Cloning and Expression of the InvA Gene

(A and B) DNA blot analysis of BssHII-digested DNAs of CRH22, InvA1 and three revertants of InvA1. A 2.7 kb fragment (between the dots) was detected in InvA1 in a blot probed with *Jordan* (A). When genomic DNA from this fragment (JFS) was cloned and used to probe a similar blot (B), a 2.7 kb fragment was again detected in InvA1 DNA. As predicted (because *Jordan* is 1.6 kb long), 1.1 kb fragments were detected in CRH22 and two of the revertants. In the other revertant, however, a larger fragment was found, indicating that *Jordan* had excised imprecisely.

(C) Genomic and cDNA maps of *invA*. The 15.3 kb lambda clone, 61λG2, which was recovered from a genomic library probed with JFS, was able to rescue InvA by transformation. Sequencing revealed that part of it (white box) encoded a kinesin motor domain. Arrows indicate where *Jordan* insertions were found in InvA1 and two other mutants (InvA2 and InvA3). The ~3.8 kb coding region of *invA* was defined by a combination of cDNA cloning, RT-PCR and 5′RACE and was found to comprise 22 exons. A typical volvocacean polyadenylation signal (TGTAA) was located 18 nt upstream of the poly(A) tail.

(D) The *invA* gene encodes a kinesin-like protein with a conserved NH_2-terminal motor domain, a predicted coiled-coil intermediate domain, and a C-terminal tail domain with no known sequence homologies. The putative InvA protein is 1003 residues long with an estimated molecular mass of 107 kDa and a pKI of 5.17.

(E) Aligned amino acid sequences of the motor domains of chicken chromokinesin, mouse Kif4, *V. carteri* InvA, and *C. reinhardtii* Iar1. Boldface indicates residues that are identical in at least 3 of these 4 sequences. Solid boxes and letters identify the eight conserved motor-domain motifs (A–F, X and Y), and asterisks within these boxes identify residues conserved in most kinesins. The dashed box identifies a WD40 motif (with "+" signs above the W and D) that is present in InvA and Iar1, but has not yet been found in any other kinesin.

(F) A comparison of mutant and wild-type RNAs. An ~3.8 kb *invA* transcript is seen in RNA from inverting wild-type embryos, but no signal is detected with equivalent RNA from the InvA1 mutant. (C38 is a constitutively expressed transcript that is used as a loading control.)

(G and H) Stage-specific *invA* expression in wild-type embryos. RNAs from uncleaved gonidia, from embryos at the five stages indicated, and from juveniles beginning their "expansion" phase are compared (G). The signals on the two Northern blots shown in (G) were quantified by densitometry, the C38 readings were used to normalize the *invA* values, and the resulting normalized values were plotted as a function of time after the beginning of embryogenesis (H). Note that *invA* expression is maximal in inverting embryos.

the entire embryo, so it is clear that it is the cells that move relative to their cytoplasmic bridges, and not the reverse; Green et al., 1981; Viamontes et al., 1979). This inward movement causes the cells to go from being linked to their neighbors at their widest points to being linked at their narrow, outermost tips (Figure 2B), which in turn forces the cell sheet to bend sharply backward over itself.

SEM examination of inversion-arrested InvA embryos revealed that the mutant cells had changed shape normally, but had not moved normally, so they all remained linked near their midpoints (compare Figures 2B and 2D). By itself, the change in cell shape (from spindle to flask) apparently was adequate to cause the cell sheet to curl outward loosely, but it was not adequate to cause formation of a normal acute, self-propagating bend region.

Time-lapse video microscopy of isolated cell pairs provided a more dynamic view. In the wild-type pair shown in Figure 2E, after the cells became flask-shaped they moved relative to their common attachment point (the cytoplasmic bridge region) until they became linked only at their chloroplast ends. In contrast, in the InvA cell pair shown in Figure 2F, although both cells became flask-shaped, neither cell ever moved with respect to the cytoplasmic bridge region that linked them. Therefore, when the long extensions of these flask cells were withdrawn at the end of the sequence shown, the cells were still connected at their equators.

We conclude that the InvA mutant fails to invert because its cells fail to move relative to the cytoplasmic bridge system that links them to their neighbors.

The *invA* Gene Encodes a Kinesin

When *Jordan* was used to probe a DNA blot containing BssHII-digested DNAs of CRH22, InvA, and three InvA revertants, a 2.7 kb fragment was detected in InvA but not the other strains (Figure 3A). We cloned this fragment and isolated from it the "*Jordan*-flanking segment" (JFS) of genomic DNA. JFS detected the same 2.7 kb fragment of InvA DNA that *Jordan* did (Figure 3B), but the fragments it detected in CRH22 and two revertants were shorter by 1.6 kb (the size of *Jordan*). Interestingly, in the third revertant (Rev2) the JFS-positive fragment was ~0.4 kb longer than in CRH22, indicating that in Rev2 *Jordan* had excised imprecisely.

Transformation of InvA with 61λG2, a JFS-positive genomic clone, resulted in phenotypic rescue. So then rescue experiments with 61λG2 fragments were used to define the maximum extent of the *invA* gene (Figure 3C). Sequencing revealed that 61λG2 included a region encoding a kinesin motor domain (open rectangle in Figure 3C). After the *invA* transcript was defined by RT-PCR, we found that its coding region comprised 22 exons and 21 introns (Figure 3C) and encoded a kinesin with an N-terminal motor domain (residues 1–420), a predicted coiled-coil stalk (420–500) and a C-terminal tail (500–1000; Figure 3D). We later found that two other mutants with the InvA phenotype had *Jordan* insertions in *invA* (Figure 3C), so we renamed the original mutant InvA1 and named the others InvA2 and InvA3.

An ortholog of InvA, which we call *iar1* (*invA*-related-1), was found in *Chlamydomonas reinhardtii*, the closest unicellular relative of *V. carteri*, by screening the *C. reinhardtii* EST database (Asamizu et al., 2000). Upon completing the sequence of *iar1* we found that it encodes a polypeptide that is >90% identical to InvA in the motor domain and C-terminal regions and is 82% identical overall (Figure 3E). Phylogenetic analysis of all 149 known kinesin motor domains (not shown) indicated that InvA and Iar1 were most similar to the KIF4/chromokinesin proteins, but the bootstrap value (~40%) was too low to provide reliable support for such a relationship, and neither InvA nor Iar1 exhibits any significant similarity to any other kinesin outside of the motor domain. Furthermore, InvA and Iar1 motor domains were both found to contain a WD40 motif of unknown significance that is not found in other kinesins. We believe that *invA* and *iar1* identify a previously unrecognized branch of the kinesin family tree.

Expression of *invA* Is Upregulated during Embryogenesis

A transcript of expected size (~3.8 kb) was detected when a Northern blot of RNA from inverting wild-type embryos was probed with an *invA* cDNA fragment, but no transcript was detected in RNA from InvA1 embryos (Figure 3F) or InvA2 or InvA3 embryos (data not shown). Thus, all three of these strains are essentially null mutants. Developmental Northern blots of wild-type RNA revealed that *invA* expression is strongly upregulated during embryogenesis, and that transcript levels are maximal during inversion (Figures 3G and 3H).

Strain InvA2-HA6B, was generated by transformation rescue of mutant InvA2 with a plasmid encoding an HA(hemagglutinin)-tagged InvA protein (Figure 4). Western blots of stage-specific extracts of InvA2-HA6B stained with an anti-HA monoclonal revealed that accumulation of the protein followed a time course similar to the transcript accumulation pattern seen on Northern blots (Figure 4D).

InvA Is Localized in the Cytoplasmic Bridge Region

The localization of HA-InvA in InvA2-HA6B was studied by IF (indirect immunofluorescence) of embryos double-stained with anti-HA and anti-tubulin antibodies. In preinversion embryos the anti-HA signals are located halfway between the basal body (inner) and chloroplast (outer) ends of cells throughout the entire embryo (Figure 5A). An optical cross-section through these cells in the region where their HA signal is most intense (Figure 5E) reveals that the antigen is localized in a punctate reticular network that is closely associated with the ring of cortical microtubules that is known to outline each cell of an inverting embryo (Green et al., 1981; Viamontes et al., 1979). This pattern is consistent with the hypothesis that InvA is associated with the cytoplasmic bridges in preinversion cells.

In early-inversion embryos, the anti-HA signal remains in its preinversion location in cells near the posterior pole of the embryo. However, in cells progressively closer to the bend region, the HA signal is located progressively closer to the outer, chloroplast ends of the cells (Figure 5B). Most importantly, in cells within the bend region—where the cytoplasmic bridges are known to be at the outermost tips of the flask cells—the InvA signal is lo-

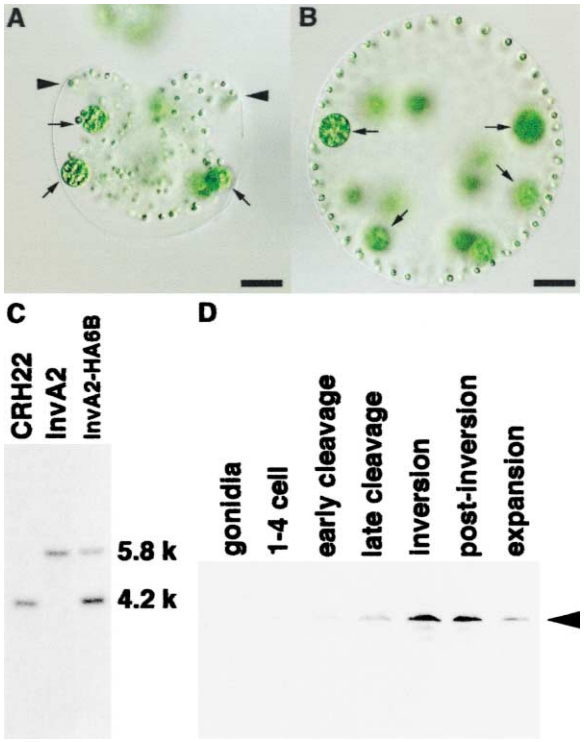

Figure 4. Rescue of an InvA Mutant with a Tagged Transgene

(A) Strain InvA2, which has a *Jordan* insertion in an *invA* intron (see Figure 3C), has the same inversion phenotype as InvA1 (cf. Figure 1B). The arrowheads indicate the edges of the partially inverted somatic-cell layer and the arrows point to some of the gonidia that remain on the outside. Scale bar is equal to 10 μm.

(B) InvA2-HA6B, a morphologically wild-type strain that was produced by transforming InvA2 with a transgene encoding HA-tagged InvA. Scale bar is equal to 10 μm.

(C) DNA blot analysis of the *invA* genes of strain InvA2, InvA2-HA6B and its progenitors in a KpnI digest. A 4.2 kb *invA*-positive band is detected in CRH22, but in InvA2 the fragment is 5.8 kb, due to the 1.6 kb *Jordan* insertion. InvA2-HA6B retains the 5.8 kb band of InvA2, but also has a 4.2 kb transgene.

(D) Western blot analysis of HA-InvA levels in InvA2-HA6B embryos. Anti-HA antibody detects a single ~140 kDa band (arrowheads) that appears in early cleavage, reaches maximum abundance during inversion, and then slowly declines, paralleling the abundance pattern seen for the corresponding mRNA (Figures 3G and 3H).

cated at the outermost tips of the cells (Figures 5B and 5C). This pattern is consistent with the hypothesis that InvA remains associated with the cytoplasmic bridges as the bend region is generated. Indeed, the staining pattern of an early-inversion embryo (Figure 5B) is strongly reminiscent of a drawing published many years ago (Green et al., 1981), indicating the location of the cytoplasmic bridge system in such embryos (Figure 5F).

In postinversion embryos, when the cells have assumed a columnar shape and are linked to their neighbors only at their chloroplast (now innermost) ends, the HA signal also is found exclusively at the chloroplast ends of the cells (Figure 5D)—again consistent with the hypothesis that InvA is associated with the cytoplasmic bridges.

Improved resolution was obtained when two-cell fragments of HA-tagged embryos were examined by anti-HA IF. In preinversion cells the antigen was restricted to the cellular equator where the cells were attached to one another (Figure 6A). In midinversion cells the antigen was located near the ends of the elongated stalks at the chloroplast ends of the cells (Figure 6B). In postinversion cells the antigen remained near the chloroplast end, in the zone where the cells were attached to one another (Figure 6C).

Still higher resolution was obtained by EM-level immunolocalization. Immunogold particles were selectively located near the bases of the cytoplasmic bridges (Figures 6D and 6E) which is where previous ultrastructural studies have shown that the plasmalemma is coated with a series of concentric cortical striations and is closely associated with a parallel array of cortical microtubules that run parallel to the long axis of the stalk (Green et al., 1981).

Discussion

The Importance of the *Jordan*-Tagging System for Analyzing *Volvox* Development

Although many chemically induced inversion mutants of *V. carteri* were isolated and described 20–30 years ago (Kirk et al., 1982; Sessoms and Huskey, 1973), attempts to use them to define the genetic program for inversion foundered for two reasons: the morphological defects of the mutants precluded mating and Mendelian analysis, and ways were not found for defining the primary mutant defects. The development of a transposon-tagging system, using the *Volvox* transposon *Jordan* (Miller et al., 1993), solved both problems: the fact that many *Jordan*-induced mutations can be induced to revert with high frequency makes it possible to circumvent Mendelian analysis and establish the causal relationship between a particular *Jordan* insertion and a mutant phenotype more directly. Then the transposon tag facilitates cloning and characterization of the affected locus. Two loci that play key roles in germ-soma differentiation of *Volvox* had been analyzed this way previously (Kirk et al., 1999; Miller and Kirk, 1999).

Here, we isolated ~50 mutants with inversion defects, of which 10 were revertible at low temperature, and of which three (InvA1, A2, and A3) turned out to have *Jordan* insertions in the same gene: *invA*, which we have now cloned and characterized.

The Role of InvA in the Movement of Flask Cells Relative to the Cytoplasmic Bridge System

Earlier ultrastructural and experimental studies of *Volvox* inversion (Green et al., 1981; Viamontes et al., 1979) led to the following two-part hypothesis to account for the formation of the bend region where the cell sheet folds outward and back over itself: (1) the cytoplasmic bridge system that links all cells of a *Volvox* embryo provides the only structural framework against which the cells can exert force; (2) the force necessary to bend the sheet outward is generated by the flask cells as they move inward relative to the cytoplasmic bridge system, and thereby go from being linked to their neighbors at their widest point to being linked at their narrowest, outermost ends (Figure 2B).

What might be the molecular basis for such a forceful

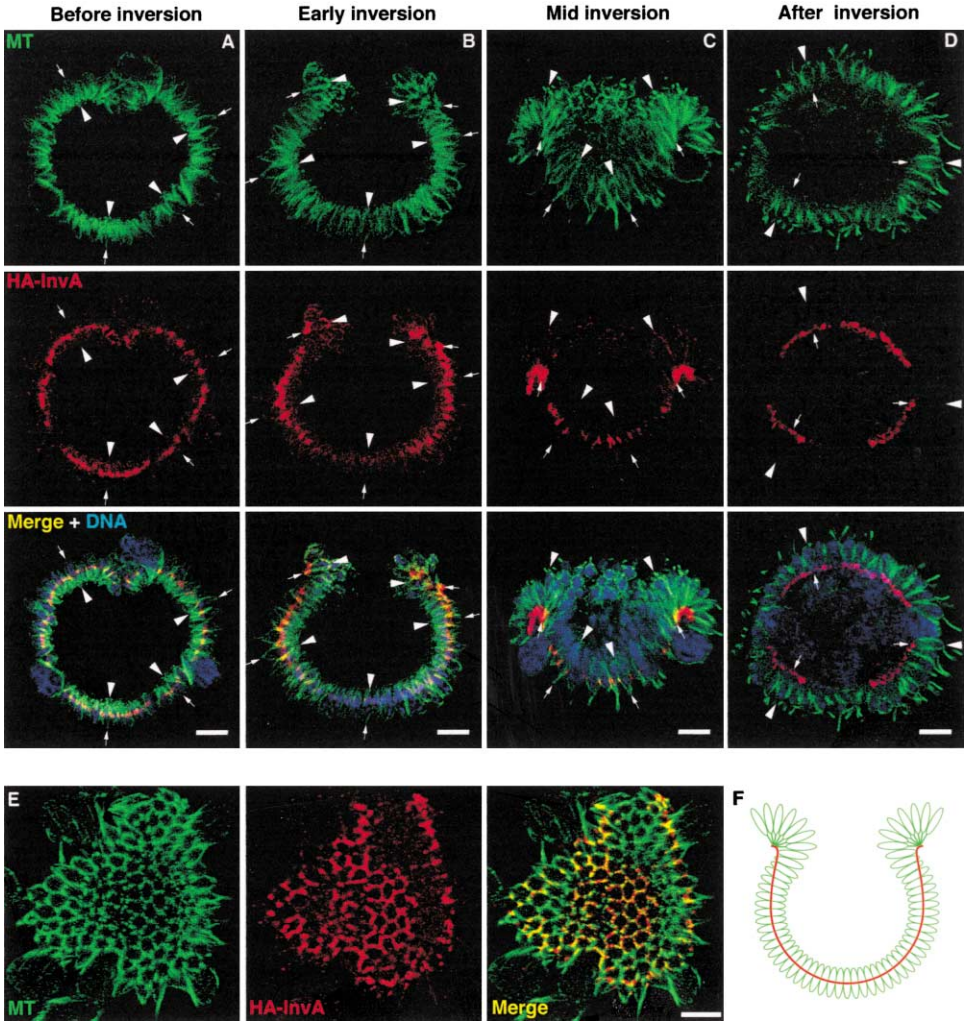

Figure 5. Indirect Immunofluorescent Analysis of InvA Localization

(A–D) Sagittal optical sections obtained by confocal microscopy of InvA2-HA6B embryos labeled with anti-tubulin (top row), anti-HA (second row), and with both primary antibodies plus TOTO-3, a DNA stain (third row). In each frame, the full lengths of several representative cells are indicated by an arrowhead marking the basal body end and a small arrow marking the chloroplast end of that cell. Cortical microtubules line the cell boundaries at all stages, and in later stages flagellar microtubules are also present. Before inversion (A) the HA-InvA signal is located near the cell equator (halfway between arrows and arrowheads). In early inversion (B) and midinversion (C), the signal remains near the equator of cells in the posterior hemisphere, but it is now at the outer, chloroplast end of cells in the bend region (see arrows in the bend region). After inversion (D), InvA is still located at the chloroplast ends of all cells, but now the chloroplast ends of the cells are on the inside of the embryo. Scale bar is equal to 10 μm.

(E) A tangential optical section through the cytoplasmic bridge region of cells in the posterior hemisphere of a midinversion embryo, perpendicular to the plane shown in (B). In this plane it is seen that InvA is closely associated with the ring of cortical microtubules that girdles each cell, and that neither of these antigens is detected deeper in the cytoplasm. Scale bar is equal to 10 μm.

(F) A diagrammatic representation of the cytoplasmic bridge system in an early-inversion embryo, adapted from the diagram in Green et al. (1981). Cell outlines are shown in green and the cytoplasmic bridge system is represented as a red line running through all of the cells. Note the similarity to the InvA staining pattern seen in (B) and (C).

movement of flask cells? Early experiments led to the conclusion that this movement was actomyosin dependent (Viamontes et al., 1979). However, a more recent study led to a different conclusion: that actomyosin plays an important role in the propagation of the bend region from the anterior into the posterior hemisphere of the embryo, but not in the movements of individual flask cells or initial generation of the bend region (Nishii and Ogihara, 1999). It was thus suggested that these movements might be microtubule-mediated.

Here, we provide evidence that in the absence of a functional InvA kinesin, the cells change shape normally, but do not move normally relative to the cytoplasmic bridge system (Figures 2D and 2F). As a consequence, a sharp bend region is never formed, and inversion stops at an early stage (as diagrammed in Figure 7B).

In Figure 7C, we provide a model indicating how we believe that the InvA kinesin may function. It has been clearly shown that all cells of an inverting *Volvox* embryo contain numerous cortical microtubules that originate near the basal bodies, and that traverse the cell just below the plasmalemma, passing very close to the cyto-

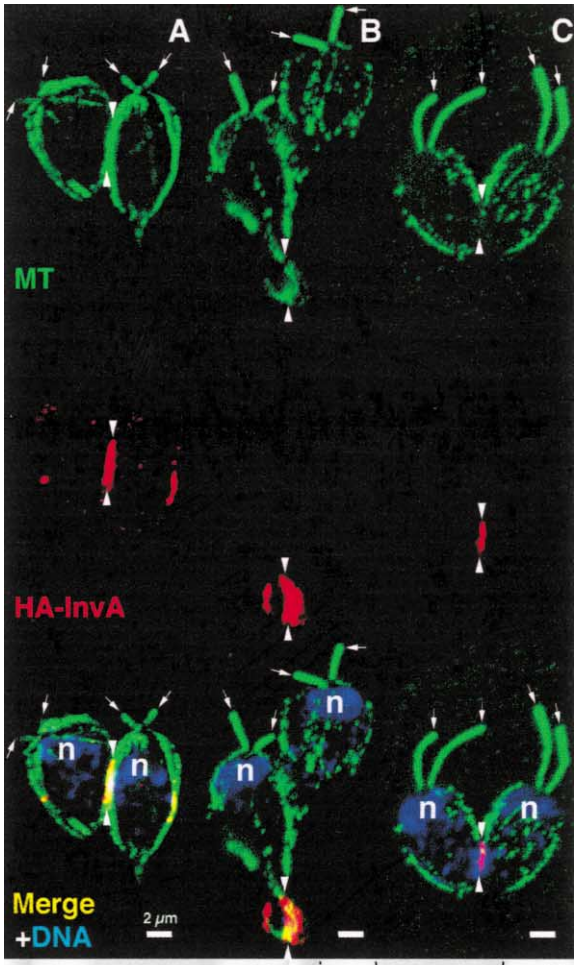

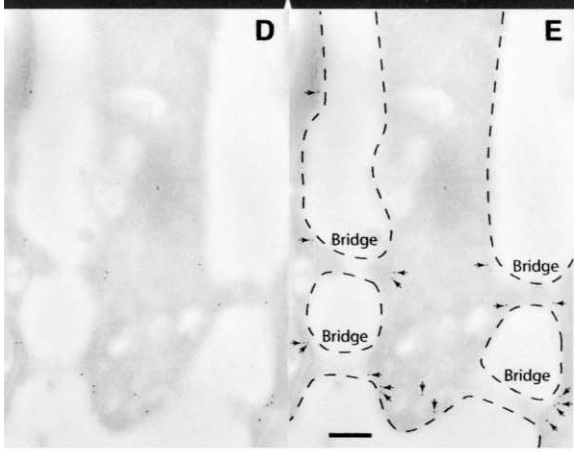

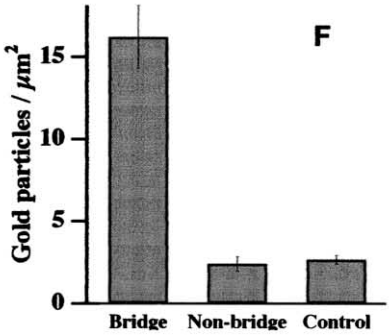

plasmic bridges, and terminating at the extreme tips of the flask-cell stalks (Green et al., 1981; Viamontes et al., 1979). Here, we have shown that the InvA kinesin, which we postulate is a plus end-directed microtubule motor as other kinesins with an N-terminal motor domain are (Hasson and Cheney, 2001), is located at the bases of the cytoplasmic bridges (Figures 6D and 6E) where previous studies have revealed that there are a number of cortical specializations that appear to link the bridges and that account for the structural integrity of the bridge system (Green et al., 1981). We propose that when InvA molecules are activated in the bridge region of flask cells, they attempt to move along the adjacent microtubules toward their the plus (outer) ends (red arrows). But because the InvA molecules are anchored in the bridge region, they cannot move downward to any significant extent. Instead, the force they exert causes the microtubules, and consequently the entire cell, to move upward (green arrow). Inhibition of GFP-InvA by microscale chromophore-assisted laser inactivation may provide a means of testing this working hypothesis in the future (Rajfur et al., 2002; Surrey et al., 1998).

In the screen that identified three Inv mutants with *Jordan* insertions in the *invA* gene (InvA1, 2 and 3), four other highly revertible mutants with an InvA-like phenotype were identified that have no detectable lesion in the *invA* gene (data not shown). Characterization of these mutants may lead to identification of molecules with which the C-terminal region of InvA (its proposed tail) interacts. And this, in turn, might provide important additional insights into the way that InvA is localized and/or executes its function.

How Does a Program for Multicellular Morphogenesis Evolve?

It is only ~50 million years since *Volvox* and several genera of volvocacean algae of intermediate size and complexity all shared a common ancestor with unicellu-

Figure 6. InvA Localization at Higher Resolution

(A–C) Two-cell fragments of InvA2-HA6B embryos. Spindle-shaped preinversion cells (A), flask-shaped midinversion cells (B), and columnar postinversion cells (C) were triple-stained as in Figure 5. Arrows indicate the flagella, which elongate during and after inversion; "n" indicates the nuclei. In spindle-shaped preinversion cells (A), HA-InvA (red) is located near the cell equator (arrowheads). In flask cells from an inverting embryo, however, the antigen is found at the extreme chloroplast ends of the cells (B). The antigen remains near the chloroplast ends of postinversion cells (C). Scale bar is equal to 2 μm.

(D–F) EM-level immunogold localization of HA-InvA in the tip of an elongated flask cell of InvA2-HA6B that is linked to its neighbors by four cytoplasmic bridges. In (E) dashed lines and small arrows have been added to the micrograph shown in (D) to highlight the location of the cell boundaries and the immunogold particles, respectively. Note that the gold particles are associated predominantly with the inner ends of the cytoplasmic bridges. Scale bar is equal to 250 nm.

(F) Quantitation of immunogold labeling. Bars indicate means ± standard errors. Bridge: particle density within 500 nm of the cytoplasmic bridges in InvA2-HA6B flasks cells. Non-bridge: particle density in the same cells in regions >500 nm from the nearest bridge. Control: particle density in bridge and non-bridge regions of wild-type embryos that lack the HA tag, but that were labeled with anti-HA and immunogold in the same way.

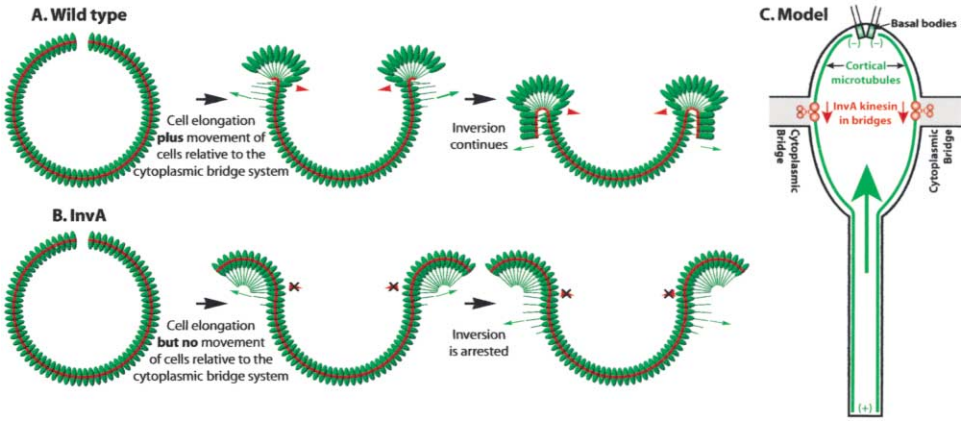

Figure 7. The Role of InvA in *V. carteri* Inversion

(A and B) Diagrammatic representations of inverting embryos viewed in midsagittal section. The gaps at the top of the embryos on the left represent the phialopore and the red line represents the cytoplasmic bridge system that links all of the cells.

(A) In wild-type embryos the force necessary to fully invert the embryo is generated by a change in cell shape accompanied by active movement of cells. The cells become flask shaped by forming long, narrow projections from their outer ends (green arrows); then they move inward relative to the cytoplasmic bridge system (red arrowheads) until they reach the point where they are linked only at their narrow outermost tips. Together these actions produce an acute bend region where the cell sheet is folded back on itself very tightly. Then as cells that have been within the bend region assume simple columnar shapes, and flask cells further from the phialopore move relative to the cytoplasmic bridge system, the bend region is propagated toward the posterior pole.

(B) In the absence of the InvA kinesin the cells transform from spindle-shaped to flask-shaped, but they fail to move relative to the cytoplasmic bridges. By itself the change in cell shape is sufficient to allow the edge of the cell sheet to curl outward loosely, but it is inadequate to produce the self-propagating, acute bend region that is required to complete inversion.

(C) Our model for the way that InvA drives inversion. This drawing represents a flask cell that is about to move with respect to the cytoplasmic bridges that link it to its neighbors. The green lines represent the numerous cortical microtubules (MTs) that are known to run from the vicinity of the basal bodies, past the cytoplasmic bridges, and to the tip of the stalk. Their polarity is indicated by the symbols (+) and (−). The InvA kinesin (which the sequence indicates is probably a plus-end-directed MT motor) is shown attached to the cytoplasmic bridges, as indicated by Figures 5 and 6. Our working hypothesis is that as InvA kinesin molecules in the cytoplasmic bridges are activated in flask cells, each attempts to move down an adjacent cortical MT toward its plus end (downward-directed red arrows). However, since each bridge is part of a coherent "bridge system" that runs throughout the entire embryo, individual bridges are not free to move. Instead, the force that is produced as many kinesin molecules try to move toward the plus ends of many cortical MTs results in a force driving all of the MTs, and hence the cell body, upward past the cytoplasmic bridges.

lar *Chlamydomonas reinhardtii* (Kirk, 1998). All of the volvocaceans, even tiny ones with only 4–16 cells, undergo a process resembling *Volvox* inversion after completing embryonic cleavage. Obviously, however, *Chlamydomonas*, being a unicell, has no need for any such multicellular morphogenetic process. Yet it possesses a gene (*iar1*) that encodes a kinesin extremely similar to InvA (Figure 3E). This raises several interesting questions: what is the subcellular function of the Iar1 kinesin in *Chlamydomonas*? How early in Volvocacean evolution was this kinesin coopted for a new role in multicellular morphogenesis? Did the evolutionary changes permitting it to take on this new role occur within the kinesin-encoding gene itself? Or within genes encoding other molecules with which InvA interacts? We hope to address these and certain other related questions experimentally in the foreseeable future.

Experimental Procedures

Volvox Strains and Cultivation Conditions

V. carteri cultures were maintained in standard *Volvox* medium (SVM) at 32°C, under the standardized conditions and light-dark cycle that synchronizes development (Kirk and Kirk, 1983, 1985). EVE (Adams et al., 1990) is a subclone of HK10, the standard female of *V. carteri* (Starr, 1969, 1970). CRH22 is a morphologically wild-type, Nit^- (reduced nitrogen-requiring) derivative of EVE (Miller et al., 1993). Cultures to be screened for mutants were held for 7–10 days at 24°C, which is near the lower limit for growth of *V. carteri*, and which stimulates transposition of the *Jordan* transposon (Miller et al., 1993). Reduced nitrogen was omitted from the medium that was used to select Nit^+ transformants.

Isolating and Characterizing Inversionless Mutants

Mutants were isolated from 24°C incubated CRH22 cultures in a multistep procedure.

Phototactic Enrichment

Unidirectional light was used to deplete a *Volvox* culture of normal individuals and enrich it in uninverted individuals and others with defects that prevent phototaxis (Sessoms and Huskey, 1973), as follows: organisms were collected by filtration and placed at one end of an SVM-filled glass chromatography tube that was then sealed and left for several hours in a room lit only by an 8W fluorescent light above opposite end of the tube. Organisms at the dark end of the tube were then collected, cultured under standard conditions for 2 days, harvested, and subjected again to phototactic enrichment.

Identification and Characterization of Mutants

Organisms from the dark end of the tube were examined with a dissection microscope and individuals with inversion abnormalities were cultured separately for several asexual generations to determine the stability and heritability of their inversion defects. Strains with heritable defects were tested for phenotypic reversion at 24° and 32°C (Miller et al., 1993) and strains with enhanced reversion at 24°C were subjected to extensive RFLP analysis as previously described (Miller and Kirk, 1999). DNA from each mutant, its progenitor (CRH22), and several of its revertant progeny was examined in a DNA blot that was hybridized with the *Jordan* transposon, looking

for *Jordan*-positive fragments present in the mutant but missing from both the progenitor and the revertant progeny.

Based on such an analysis, we selected for study a strain with a 2.7 kb *Jordan*-positive BssHII restriction fragment not present in CRH22. We named it InvA and defined the *invA* locus as the one bearing a lesion in strain InvA. Later two more mutants were found with *Jordan* insertions in the *invA* locus, so they were named InvA2 and InvA3 and the original mutant was renamed InvA1.

Preparation of an *invA* Genomic Clone

The 2.7 kb *Jordan*-tagged BssHII restriction fragment of InvA1 was cloned, and genomic DNA flanking the *Jordan* insertion in it was isolated, all as previously described (Kirk et al., 1999). This *Jordan*-flanking segment (JFS) was used to screen a genomic library of randomly sheared EVE DNA in λ Dash II (Stratagene, La Jolla, CA), yielding two overlapping genomic clones that were sequenced. One of these clones (61λG2, Figure 3C) was used for phenotypic rescue of InvA mutants, indicating that it contained all the information required to restore *invA* function.

Nuclear Transformation

The ability of genomic clones to rescue InvA mutants was tested by biolistic cotransformation, using the *nitA* gene as the selectable marker, as previously described (Kirk et al., 1999). Bombarded samples were cultured in selective medium in multi-well plates and monitored for the appearance of green, growing (Nit^+) survivors, each of which was cultured separately and scored for its inversion phenotype. No more than one wild-type strain was saved per initial culture well. Each putative cotransformant was analyzed to determine whether it contained both the mutant *invA* gene with a *Jordan* insertion and a transgene.

cDNA Cloning and RT-PCR Analysis of the *invA* Transcript

A cDNA library made from RNA of *V. carteri* embryos was screened with JFS. The only clone recovered had a 1 kb insert that contained a poly(A) tail and 3′ UTR, but no significant open reading frame. Therefore, RT-PCR was used to complete the analysis of the *invA* transcript.

RT was performed with the Omniscript RT kit (Qiagen), using three different oligonucleotides (from Integrated DNA Technologies, Coralville, IA) that were designed to serve as primers for reverse transcription of the C-terminal coding region, the N-terminal coding region and the 3′ UTR. (Sequences of all RT and PCR primers available on request.) First-strand cDNAs were amplified by PCR, using Taq DNA polymerase (Promega, Madison, WI) and three forward primers designed on the basis of the kinesin sequence we found in the genomic clone. The 5′-RACE method was performed by standard methods (Sambrook and Russell, 2001).

Analysis of the *Chlamydomonas* Ortholog of InvA, Iar1

We completed the sequencing of four clones we found with InvA-related sequences in the *C. reinhardtii* EST library of Kazusa DNA Institute, Japan (Asamizu et al., 2000) (GenBank accession numbers AV628397, AV626304, AV644452 and AV626877) and found that they contained overlapping portions of a single gene we named *iar1* (for *invA*-related-1). The deduced amino acid sequences of the kinesin motor domains encoded by *invA* and *iar1* were aligned with all 147 available kinesin sequences (http://www.proweb.org/kinesin//) using ClustalW (Thompson et al., 1994).

Northern Blots

A Northern blot was prepared as described (Tam and Kirk, 1991) with RNA from 4–5 × 10^5 synchronous embryos at each stage of interest, and was probed with 1.2 kb DNA fragment encoding the carboxyl half of the *invA* motor region. Blots were hybridized in PerfectHyb Plus Hybridization buffer (Sigma, St. Louis, MO) containing 10 μg/ml of salmon sperm DNA (Sigma) at 68°C for 24 hr and the final wash was with 0.2 × SSC, 0.1% SDS.

Protein Studies Using Hemagglutinin-Tagged InvA

A plasmid carrying the *invA* genomic sequence was modified by inserting DNA encoding the hemagglutinin (HA) epitope (Jarvik and Telmer, 1998) into a *Drd* I site at the end of the 14th exon and was then used to transform strains InvA1 and A2. Following DNA blot analysis, the transformant with the fewest copies of the HA-InvA transgene copies (InvA2-HA6B; Figure 4C) was selected for further study.

Extracts of InvA2-HA6B for Western blots were prepared as previously described (Kirk et al., 1999), using Coomassie brilliant blue staining to assure equal loading. Proteins were transferred to ImmunoBlot PVDF Membrane (Bio-Rad, Hercules, CA) using Towbin buffer with 0.1% SDS (Towbin et al., 1979); the membrane was blocked with TBS containing 0.1% tween-20 and 3% nonfat dried milk and then incubated with an anti-HA mouse monoclonal antibody (McAb; 12CA5, 1:5000). Immunoreactivity was visualized with HRP-linked sheep-anti-mouse antibody (1:10,000; Amersham Biosciences, Piscataway, NJ) in blocking solution plus SuperSignal Chemiluminescent Substrate (Pierce Biochemicals, Rockford, IL).

InvA2-HA6B embryos for immunocytology were attached to coverslips precoated with polyethylenimine (PEI; Sigma) and prepared for IF analysis as described (Nishii and Ogihara, 1999), except for the addition of a 1 hr postfixation in 3.7% formaldehyde after chlorophyll extraction. The primary antibodies used were 1:1000 12CA5 and 1:1000 rat anti-α tubulin McAb (provided by S. Miller) and the secondary antibodies were 1:300 Alexa Fluor 488 goat anti-rat IgG and 1:300 Alexa Fluor 568 goat anti-mouse IgG (Molecular Probes, Eugene, OR). DNA was stained with 0.2 μg/ml TOTO-3 (Molecular Probes). Confocal images were obtained with a Leica TCS SP2 system.

Video Microscopy of Isolated and Fragmented Embryos

Whole embryos attached to PEI-coated coverslips were observed and recorded as previously described (Nishii and Ogihara, 1999). Fragmented embryos (obtained by passing embryos in and out of a 10 μl Hamilton glass syringe 3–5 times) were examined by DIC, using a Plan Fluor 100×/1.3 objective on an Eclipse E600 microscope (Nikon, Kawasaki, Kanagawa, Japan). Time-lapse images were captured with a Nikon digital camera DN100 and analyzed with the NIH ImageJ 1.29 (http://rsb.info.nih.gov/ij/) and Adobe Photoshop 7 (San Jose, CA) software.

Scanning and Transmission Electron Microscopy

Embryos were prepared for SEM as described (Green and Kirk, 1981), and examined with a Hitachi S-450 SEM. Samples of InvA2-HA6B and EVE (control) embryos were prepared as described for EM-level immunolocalization (Hallmann and Kirk, 2000). Thin sections preincubated with 1:100 12CA5 for 18 hr at 4°C were incubated with 10 nm colloidal gold particles coated with goat anti-mouse IgG (Ted Pella, Redding, CA) for 4 hr at room temperature and then stained successively with OsO_4, uranyl acetate, and lead citrate and examined in a Hitachi H-600 TEM.

The specificity of immunogold labeling of the cytoplasmic bridges of InvA2-HA6B embryos was evaluated by counting gold particles within a 500 nm circle centered on the base of each cytoplasmic bridge, in the remainder of these same cells, and in control (EVE) cells that lack the HA tag.

Acknowledgments

We thank S. Miller for guidance in use of the *Jordan*-tagging method, helpful discussions, and provision of antibodies; G.M. Veith for technical help with microscopy; L. Duncan for helpful discussions; K. Bouckaert, L. Rikimaru, P. Bommarito and W. Müller for technical support at various times; L. Ellis for the anti-HA McAb; and M. Kubo and T. Kakimoto for DNA sequencing. This work was supported by JSPS Postdoctoral Fellowship for Research Abroad to I.N. and by research grants from NSF (IBN-9904739 and IBN-0131565) to D.K.

Received: April 4, 2003
Revised: May 20, 2003
Accepted: May 28, 2003
Published: June 12, 2003

References

Adams, C.R., Stamer, K.A., Miller, J.K., McNally, J.G., Kirk, M.M., and Kirk, D.L. (1990). Patterns of organellar and nuclear inheritance

among progeny of two geographically isolated strains of *Volvox carteri*. Curr. Genet. *18*, 141–153.

Asamizu, E., Miura, K., Kucho, K., Inoue, Y., Fukuzawa, H., Ohyama, K., Nakamura, Y., and Tabata, S. (2000). Generation of expressed sequence tags from low-CO2 and high-CO2 adapted cells of *Chlamydomonas reinhardtii*. DNA Res. *7*, 305–307.

Green, K.J., and Kirk, D.L. (1981). Cleavage patterns, cell lineages, and development of a cytoplasmic bridge system in *Volvox* embryos. J. Cell Biol. *91*, 743–755.

Green, K.J., Viamontes, G.I., and Kirk, D.L. (1981). Mechanism of formation, ultrastructure, and function of the cytoplasmic bridge system during morphogenesis in *Volvox*. J. Cell Biol. *91*, 756–769.

Hallmann, A., and Kirk, D.L. (2000). The developmentally regulated ECM glycoprotein ISG plays an essential role in organizing the ECM and orienting the cells of *Volvox*. J. Cell Sci. *113*, 4605–4617.

Hasson, T., and Cheney, R.E. (2001). Mechanisms of motor protein reversal. Curr. Opin. Cell Biol. *13*, 29–35.

Jarvik, J.W., and Telmer, C.A. (1998). Epitope tagging. Annu. Rev. Genet. *32*, 601–618.

Kelland, J.L. (1977). Inversion in *Volvox*. J. Phycol. *13*, 373–378.

Kiehart, D.P., Galbraith, C.G., Edwards, K.A., Rickoll, W.L., and Montague, R.A. (2000). Multiple forces contribute to cell sheet morphogenesis for dorsal closure in *Drosophila*. J. Cell Biol. *149*, 471–490.

Kirk, D.L. (1998). *Volvox*: Molecular Genetic Origins of Multicellularity and Cellular Differentiation. (New York: Cambridge University Press).

Kirk, D.L., and Kirk, M.M. (1983). Protein synthetic patterns during the asexual life cycle of *Volvox carteri*. Dev. Biol. *96*, 493–506.

Kirk, D.L., and Nishii, I. (2001). *Volvox carteri* as a model for studying the genetic and cytological control of morphogenesis. Dev. Growth Differ. *43*, 621–631.

Kirk, D.L., Viamontes, G.I., Green, K.J., and Bryant, J.L. (1982). Integrated morphogenetic behavior of cell sheets: *Volvox* as a model. In *Developmental Order: Its Origin and Regulation* (*40th Symposium of the Society for Developmental Biology*), S. Subtelny and P. B. Green, eds., pp. 247–274.

Kirk, M.M., and Kirk, D.L. (1985). Translational regulation of protein synthesis, in response to light, at a critical stage of *Volvox* development. Cell *41*, 419–428.

Kirk, M.M., Stark, K., Miller, S.M., Muller, W., Taillon, B.E., Gruber, H., Schmitt, R., and Kirk, D.L. (1999). *regA*, a *Volvox* gene that plays a central role in germ-soma differentiation, encodes a novel regulatory protein. Development *126*, 639–647.

Kuschakewisch, S. (1923). Zur Kenntnis derEntwickslungsgeschichte von *Volvox*. Bull de l'Acad dSc de l'Oukraine *1*, 32–40.

Miller, S.M., and Kirk, D.L. (1999). *glsA*, a *Volvox* gene required for asymmetric division and germ cell specification, encodes a chaperone-like protein. Development *126*, 649–658.

Miller, S.M., Schmitt, R., and Kirk, D.L. (1993). *Jordan*, an active *Volvox* transposable element similar to higher plant transposons. Plant Cell *5*, 1125–1138.

Nishii, I., and Ogihara, S. (1999). Actomyosin contraction of the posterior hemisphere is required for inversion of the *Volvox* embryo. Development *126*, 2117–2127.

Rajfur, Z., Roy, P., Otey, C., Romer, L., and Jacobson, K. (2002). Dissecting the link between stress fibres and focal adhesions by CALI with EGFP fusion proteins. Nat. Cell Biol. *4*, 286–293.

Sambrook, J., and Russell, D. (2001). Molecular Cloning: A Laboratory Manual, Third Edition. (Cold Spring Harbor, NY: Cold Spring Harbor Laboratory Press.).

Schock, F., and Perrimon, N. (2002). Molecular mechanisms of epithelial morphogenesis. Annu. Rev. Cell Dev. Biol. *18*, 463–493.

Sessoms, A.H., and Huskey, R.J. (1973). Genetic control of development in *Volvox*: isolation and characterization of morphogenetic mutants. Proc. Natl. Acad. Sci. USA *70*, 1335–1338.

Starr, R.C. (1969). Structure, reproduction, and differentiation in *Volvox carteri* f. *nagariensis* Iyenger, strains HK9 and 10. Arch Protistenkd *111*, 204–222.

Starr, R.C. (1970). Control of differentiation in Volvox. Symp. Soc. Dev. Biol. *29*, 59–100.

Surrey, T., Elowitz, M.B., Wolf, P.E., Yang, F., Nedelec, F., Shokat, K., and Leibler, S. (1998). Chromophore-assisted light inactivation and self-organization of microtubules and motors. Proc. Natl. Acad. Sci. USA *95*, 4293–4298.

Tam, L.W., and Kirk, D.L. (1991). The program for cellular differentiation in *Volvox carteri* as revealed by molecular analysis of development in a gonidialess/somatic regenerator mutant. Development *112*, 571–580.

Thompson, J.D., Higgins, D.G., and Gibson, T.J. (1994). CLUSTAL W: improving the sensitivity of progressive multiple sequence alignment through sequence weighting, position-specific gap penalties and weight matrix choice. Nucleic Acids Res. *22*, 4673–4680.

Towbin, H., Staehelin, T., and Gordon, J. (1979). Electrophoretic transfer of proteins from polyacrylamide gels to nitrocellulose sheets: procedure and some applications. Proc. Natl. Acad. Sci. USA *76*, 4350–4354.

Viamontes, G.I., Fochtmann, L.J., and Kirk, D.L. (1979). Morphogenesis in *Volvox*: analysis of critical variables. Cell *17*, 537–550.

Viamontes, G.I., and Kirk, D.L. (1977). Cell shape changes and the mechanism of inversion in *Volvox*. J. Cell Biol. *75*, 719–730.